ACS OMEGA

Open Access

http://pubs.acs.org/journal/acsodf

Article

Tailoring of Silicone Urethane Methacrylate Resin for Vat Photopolymerization-Based 3D Printing of Shape Memory Polymers

Aphiwat Pongwisuthiruchte, Chuanchom Aumnate,*,⊥ and Pranut Potiyaraj*,⊥

Cite This: *ACS Omega* 2024, 9, 2884−2895

Read Online

ACCESS | Metrics & More | Article Recommendations | Supporting Information

ABSTRACT: Polydimethylsiloxane (PDMS) or silicone elastomers have garnered considerable attention in the field of medical device applications due to their superior thermal stability. However, conventional manufacturing techniques for silicone elastomers suffer from drawbacks such as cost, lengthy production time, and inherent difficulties in fabricating complex structures. To address these limitations, photosensitive polydimethylsiloxane urethane methacrylate (PDMSUMA) oligomers were synthesized, and their curing behaviors were specifically investigated for vat photopolymerization 3D printing applications. The study focused on exploring the impact of weight ratios between poly(ethylene glycol) dimethacrylate (PEGDMA) and 2-hydroxyethyl methacrylate (HEMA) in the PDMSUMA resin formulation. The addition of PEGDMA as a reactive diluent was found to enhance the printability of the PDMSUMA resin and decrease its viscosity. Thermal, mechanical, and shape memory properties of the 3D-printed specimens were examined. Our findings demonstrate the potential of PDMSUMA resins for developing customizable shape memory materials with tailored properties.

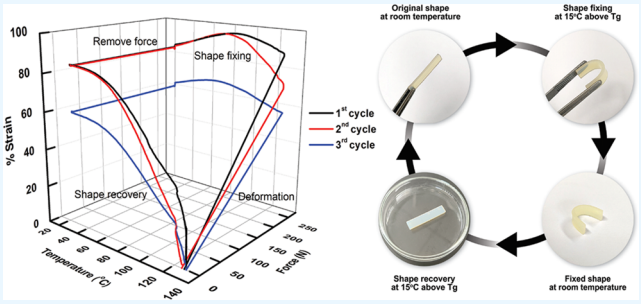

1. INTRODUCTION

Shape memory polymers (SMPs) are polymeric smart materials that can regain their original shape in response to external stimuli, such as temperature, light, electricity, magnetism, or moisture.[1−3] When compared to shape memory alloys, SMPs offer more efficient deformation performance, reduced material usage, and lower processing costs.[4] SMPs possess desirable properties, such as low density, low activation temperature, high elastic deformation, and promising biocompatibility and biodegradability. These properties enable SMPs to find applications in biomedicine, including self-tightening sutures, fasteners, and drug delivery carriers.[5−11]

Thermoplastics, thermosets, and recently developed thermal-adapt polymeric materials are commonly used in SMPs.[12−14] For many years, researchers have been drawn to thermoplastic SMPs due to their reprocessability, as well as their simplicity and freedom in chain structure and performance design. Although thermoplastic SMPs can be reprocessed, they frequently have poor shape fixity and recovery. Because of their structural stability, thermoset SMPs typically outperform thermoplastic materials in shape memory performance and endurance. However, their molding and machining techniques limit the complexity of the original shapes.

Conventionally, thermoresponsive SMPs are processed to return to their original shape. The polymer is initially deformed and then fixed in the temporary shape through a programming process involving heating, deforming, and cooling of the specimen. Heating the SMP above its transition temperature enables recovery of the stored, original shape. On cooling below the transition temperature, the material solidifies, but the temporary shape is not visible. This phenomenon is known as the one-way shape memory effect. The temporary shape can be reprogrammed through further processes, including mechanical deformation, leading to a new temporary shape.

An elastomer can exhibit shape memory functionality if it can be stabilized in a deformed state within a relevant temperature range for its intended application, which can be achieved by utilizing the network chains as a type of molecular switch, where the flexibility of the segments is temperature-dependent. One possible means of achieving this switch function is by utilizing the thermal transition of the network chains within the temperature range of interest. Above the transition temperature, the chain segments are flexible, while their flexibility is at least partially limited below this thermal transition. For a transition from the rubber-elastic or viscous state to the glassy state, the entire segment's flexibility is limited. Fixation of the temporary shape can be achieved through strain-induced crystallization of the switching segment upon cooling above the transition temperature. However, the achieved crystallization is incomplete, allowing for a certain

Received: October 22, 2023
Revised: December 12, 2023
Accepted: December 20, 2023
Published: January 3, 2024

number of amorphous chains. These crystallites prevent the segments from immediately reforming the coil-like structure and spontaneously recovering the original shape.[15]

Polydimethylsiloxane (PDMS) or silicone elastomers are widely used materials in biomedical applications due to their biocompatibility and low or nearly noncytotoxicity.[16−19] Silicone elastomers are generally fabricated through platinum-catalyzed hydrosilylation, condensation, or peroxide-initiated radical reactions. They are all thermocuring; thus, rigid molds are generally needed to fabricate final products. Traditional manufacturing technology for silicone elastomers is costly and time-consuming, and it is unable to fabricate objects with complicated structures. The emergence of the 3D printing technology has enabled the fabrication of complex structures. Thus, many researchers have been trying to fabricate silicone elastomers through inkjet, direct writing, extrusion-based, and embedded 3D printing technologies.[20−23] However, limited printing resolution remains a challenge in the existing printing methods.

By using multimaterial 3D printers, the new process for 4D-printable SMPs has been extensively demonstrated.[24,25] The placement of the materials and the designs are extrinsic elements in multimaterial printing that influence how much the SMP will alter. The interaction of various materials is prone to interfaces and differing physical qualities such as thermal expansion, which tend to cause cracks at the boundaries and reduce the endurance of the parts.[26] The development of fabricating single SMPs with stereolithography (SLA), one of the most well-known liquid-based additive manufacturing methods, has the advantage of creating parts with excellent surface finish and high resolution. Its open build environment and readily accessible resin vat allow for complete material development freedom.[27,28] However, the commercial availability of liquid resins suitable for SLA is limited and takes a long time for production. To overcome this drawback, the production of 3D objects using mask stereolithography (mSLA) was developed, which is based on the selectively controlled solidification of liquid printing materials via photopolymerization controlled by an LCD screen, in which a UV light pattern is illuminated on the printing materials in the material vat. After curing the printing materials in the pattern region to form a thickness of materials on the building plate before rising, the building plate was moved down and the cured layer was resurfaced by printing materials. This process was continued until all 3D objects were printed. Although the readily accessible polymers have shape fixity and recovery capabilities, the thermomechanical degradation of the shape memory cycle life has rarely been examined. This determines whether the polymers can fulfill the requirements of industrial applications where the resilience of the shape memory performance over several cycles is essential.[25]

In this study, a photosensitive polydimethylsiloxane urethane methacrylate (PDMSUMA) resin was synthesized and characterized for mSLA 3D printing. PDMSUMA was formulated with a mixture of PEGDMA/HEMA at different weight ratios, and a 3 wt % photoinitiator was added to create a photosensitive resin. All test specimens were 3D printed using an mSLA 3D printer, and their mechanical, thermal, and shape memory behaviors were investigated.

2. EXPERIMENTAL SECTION

2.1. Materials. Hydroxy-terminated polydimethylsiloxane (PDMS−OH, M_n ∼ 550), isophorone diisocyanate (IPDI, 98%), 2-hydroxyethyl methacrylate (HEMA, 99%), and poly(ethylene glycol) dimethacrylate (PEGDMA, M_n ∼ 750) were purchased from Sigma-Aldrich. Diphenyl(2,4,6-trimethylbenzoyl)phosphine oxide (TPO, 99%) was purchased from Tokyo chemical industry.

2.2. Synthesis of PDMSUMA Oligomers. Silicone urethane methacrylate prepolymer was synthesized with two-step polymerization. The stoichiometry of the synthesis reaction was 2:2:1 of isophorone diisocyanate (IPDI), 2-hydroxyethyl methacrylate (HEMA), and hydroxy-terminated polydimethylsiloxane. A four-necked glass reaction flask equipped with a reflux condenser and a nitrogen gas inlet system was used. PDMS was placed into the reactor, then IPDI was added dropwise with stirring at 60 °C under a N_2 atmosphere. The reaction was kept running for 2 h, and then, HEMA was added dropwise to the solution while the mixture was stirred continuously. The reaction was continued until the absorption peak of the NCO group at 2270 cm^{-1} (traced by Fourier transform infrared spectroscopy, FTIR) has disappeared. The polymerization reaction procedure and chemical structures of the final product are schematically illustrated in Scheme S1.

2.3. Resin Formulation Design. The synthesized silicone urethane methacrylate oligomers (PDMSUMA) have a high viscosity that necessitates using of a cross-linker as a reactive diluent. The cross-linkers are often acrylic monomers which can also take part in the cross-linking reaction and promote the network structure. In this study, we aimed to investigate the effects of different weight ratios of PEGDMA and HEMA in the formulated PDMSUMA resin. The PDMSUMA and diluent were mixed in a fixed weight ratio of 70:30, while the PEGDMA and HEMA were mixed in varying weight ratios, including 100:0, 90:10, 80:20, 70:30, 60:40, and 50:50. The resulting blends were characterized by their physical properties. The diluents used in this study were a combination of monofunctional (HEMA) and bifunctional (PEGDMA) acrylic monomers at different weight ratios. Synthesized PDMSUMA oligomers were mixed with combined cross-linker and TPO (3 wt %) as an initiator for 2 h. After homogeneous mixing, the PDMSUMA photopolymer resin was kept to use as our 3D printing resin.

2.4. Fabrication of 3D-Printed Specimens. A masked stereolithography (mSLA) 3D printer, Phrozen sonic mini 4K (Hsinchu, Taiwan), was used to fabricate the 3D-printed specimen. The test specimen was designed using Fusion 360 as the CAD software and Chitubox as the slicer software. The parameters for mSLA 3D printing, as detailed in Table 1, remained consistent across all of the PDMSUMA photosensitive resin formulations. Subsequently, we conducted

Table 1. mSLA 3D Printing Parameter Setup for All PDMSUMA Photosensitive Resin Formulations

parameter	value
light source wavelength (nm)	405
layer height (mm)	0.05
bottom layer count	5
lift and retract distance (mm)	6
lift and retract speed (mm/min)	60
support	enable
antialiasing	enable

https://doi.org/10.1021/acsomega.3c08102
ACS Omega 2024, 9, 2884−2895

optimization to determine the exposure time required for curing a 50 μm layer thickness.

2.5. Chemical and Physical Characterization of PDMSUMA Resins. *2.5.1. Fourier Transform Infrared Spectrometry (FTIR) Analysis.* To compare and analyze the functional group of synthesized materials, an analysis was performed using a Thermo Fisher Scientific, Nicolet iS50, Fourier transform infrared spectrometer (Massachusetts). The synthesized materials were scanned over the range of wavenumber 4000−400 cm^{-1}.

2.5.2. Nuclear Magnetic Resonance (NMR) Analysis. ^{1}H NMR and ^{13}C NMR spectra were recorded by using a Bruker 500 MHz nuclear magnetic resonance spectrometer (Massachusetts). Deuterated chloroform ($CDCl_3$) was used as a reference solvent. ^{1}H NMR and ^{13}C NMR of silicone urethane monomer and silicone urethane methacrylate monomer were recorded for confirmation of chemical structure of reaction products.

2.5.3. UV−vis Absorbance Analysis. The UV absorbance of the synthesized 3D printing materials was performed using a LabTech BlueStar B UV−vis spectrophotometer (Massachusetts) with absorbance spectra 300−600 nm in 1 nm steps by focusing on the absorbance on wavelength 405 nm that is the recommended condition for 3D printing.

2.5.4. Viscosity. The viscosities of pure PDMSUMA and formulated PDMSUMA with PEGDMA were determined using a Brookfield DV-II+ viscometer (Toronto, Canada) at room temperature.

2.6. Curing Characterization. To measure the curing depth (C_d) for plotting Jacobs working curves,[29] the formulated PDMSUMA resins were exposed to 405 nm light with 5 mW cm^{-2} intensity (E_{max}) for 10 exposure times from 1 to 10 s. After exposure, the uncured photopolymer resin was rinsed with isopropyl alcohol (IPA), and the cured film layer was carefully dried with compressed air, and the thicknesses were measured using a digital caliper with a 0.01 mm precision. For each resin composition, a straight line was fitted to the Jacobs working curve as a logarithmic-linear plot with thicknesses of cured film or C_d on the y-axis and exposure time on the x-axis. The slope of the Jacobs working curve is the penetration depth (D_p) in μm and calculation E_c by the Jacobs equations

$$C_d = D_p \ln\left(\frac{E_{max}}{E_c}\right) \quad (1)$$

2.7. Physical Characterization of 3D-Printed Specimens. *2.7.1. Dimension Accuracy.* The 3D-printed samples were subjected to precise measurements and subsequent comparison with the corresponding CAD 3D model. The measurements encompassed the total length, width, and thickness of each individual specimen.

2.7.2. Thermogravimetric Analysis (TGA). Thermal stability measurements for all formulated PDMSUMA resins were carried out using a Mettler Toledo, TGA/DSC 3+ (Greifensee, Switzerland). The 3D-printed samples were heated from 30 to 600 °C, under a nitrogen atmosphere with a scanning temperature rate of 10 K/min.

2.7.3. Thermomechanical Analysis. Thermomechanical behavior of the 3D-printed specimens was determined with dynamic mechanical analysis (DMA) using a Thermo Fisher Scientific HAAKE MARS rheometer (Massachusetts) in the DMA mode with a solid clamp. Samples were 3D printed as rectangular bars (30 mm × 6 mm × 2 mm), and the measurements were carried out at the frequency of 5 Hz with a heating rate of 5 °C min^{-1} over a temperature range of 25−200 °C. The storage modulus (E'), loss modulus (E''), loss factor ($\tan\delta$), and glass-transition temperature (T_g), defined by the temperature at the maximum in the loss factor signals of the samples, were determined.

2.7.4. Gel Content. The measurements were performed with a Soxhlet extractor using THF as a solvent for 24 h to completely remove the uncross-linked constituents. The specimens removed from the Soxhlet were dried in a vacuum oven for an hour. The average gel contents (wt %) were calculated according to eq 2, where m_0 is the initial specimen's weight and m_1 is the mass of extracted specimens after drying in an oven.

$$\text{gel content} = \frac{m_1}{m_0} \times 100\% \quad (2)$$

2.8. Investigation of Shape Memory Behavior of 3D-Printed Specimens. The shape memory behavior of the 3D-printed specimens in terms of shape fixity ratio (R_f) and shape recovery ratio (R_r) was investigated using a Thermo Fisher Scientific HAAKE MARS rheometer (Massachusetts) with a solid clamp in the creep and relaxation mode. As shown in Figure 1, the testing procedures are set as follows:

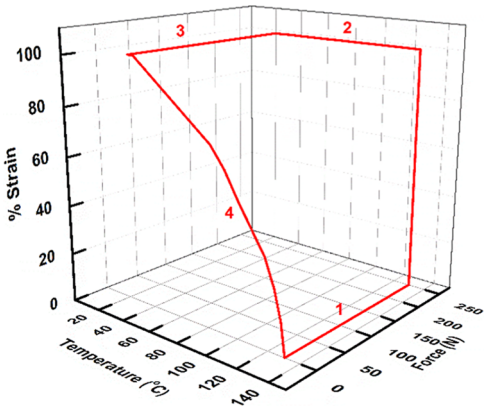

Figure 1. Diagram of a control force cyclic testing on a SMP.

(1) Heating a sample to 15 °C above T_g at a rate of 5 °C min^{-1} and maintaining isothermal for 1 min. Then deforming the sample by using creep with stress at 250 Pa for 5 min to correct strain changed.

(2) Reducing the temperature to 25 °C at a rate of 5 °C min^{-1}.

(3) Removing of force and maintaining isothermal for 5 min and then measurement of strain relaxation for 5 min.

(4) Reheating the sample at 5 °C min^{-1} to 15 °C above T_g and maintaining isothermal for 1 min and then measurement of strain relaxation for 5 min again.

(5) The test was repeated from step (1) for 3 times.

The shape fixity ratio R_f can be defined as the ability of the switching component to fix the mechanical deformation that has been applied during the programming process. It is measured as the ratio of the strain ε_u measured upon removal of the load after cooling to the strain ε_m that was applied at a temperature above T_g and N was the number of cycle

https://doi.org/10.1021/acsomega.3c08102
ACS Omega 2024, 9, 2884−2895

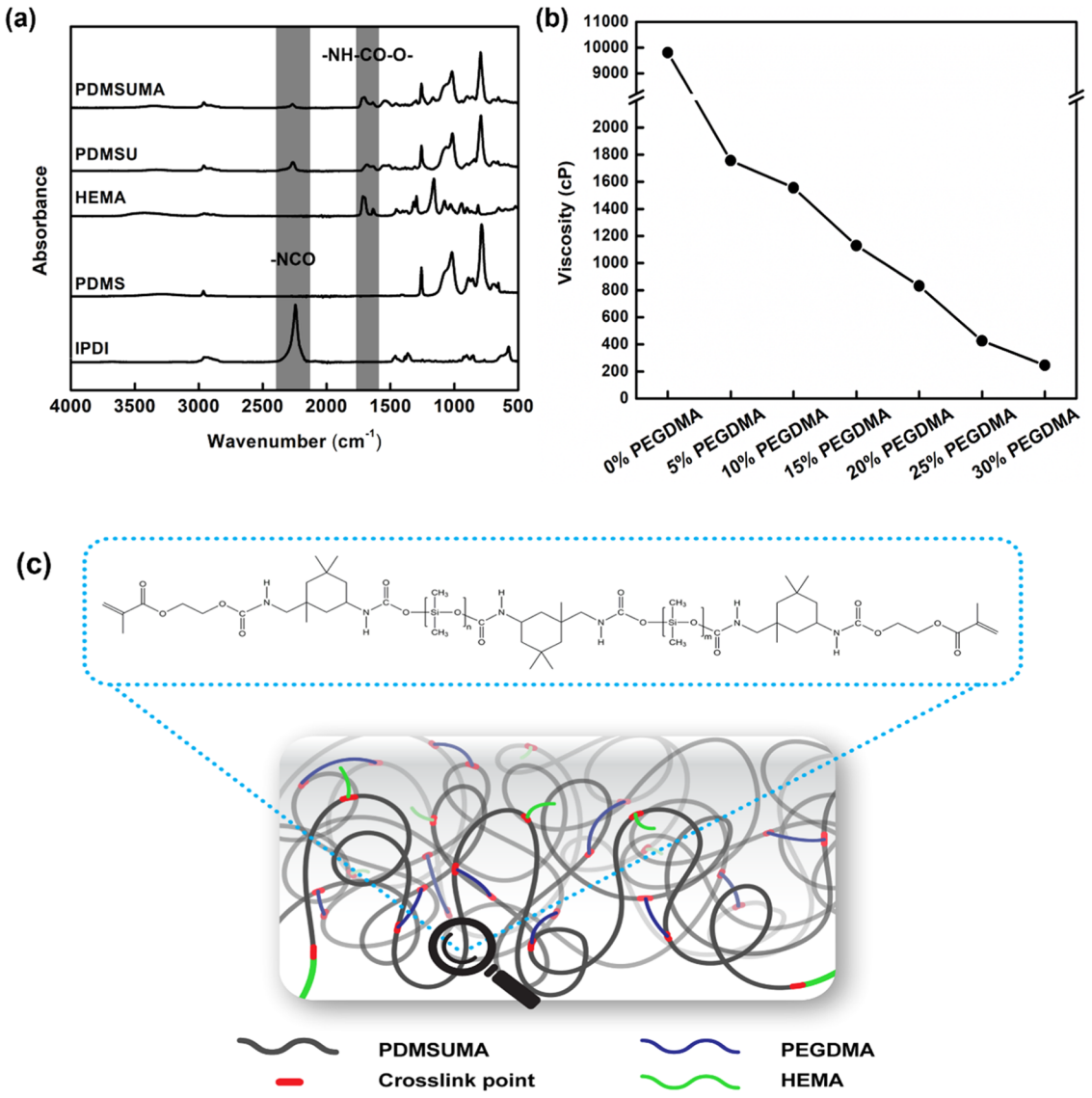

Figure 2. (a) FTIR spectra of IPDI, PDMSU, and PDMSUMA; (b) viscosity of pure PDMSUMA and formulated PDMSUMA with PEGDMA; and (c) illustrative scheme of polymerized formulated PDMSUMA with PEGDMA and HEMA.

$$R_f(\%) = \frac{\varepsilon_u(N)}{\varepsilon_m} \times 100 \quad (3)$$

The shape recovery ratio R_r quantifies the ability of the material to memorize its permanent shape and is a measure of how much applied strain is recovered upon reheating. It can also be defined as the ratio of the difference between the initial strain (ε_m) applied at the deformation step and the final strain (ε_p) measured after completion of the recovery step to the initially applied strain and N was the number of cycle

$$R_r(\%) = \frac{\varepsilon_m - \varepsilon_p(N)}{\varepsilon_m - \varepsilon_p(N-1)} \times 100 \quad (4)$$

3. RESULTS AND DISCUSSION

3.1. Characterizations of Synthesized Silicone Urethane Methacrylate (PDMSUMA) Oligomers. Figure 2a presents the FTIR spectra of the synthesized PDMSUMA and its precursors. The FTIR spectrum of IPDI showed the most intense peak at 2233.66 cm^{-1}, which is attributed to the characteristic isocyanate (−NCO) groups attached to the IPDI molecule. The NCO group is essential for the use of IPDI as an intermediate in polyurethane production. The spectrum also displayed sharp peaks at 2940 cm^{-1}, corresponding to the C−H stretching of the IPDI molecule.[30] For PDMSU and PDMSUMA, the FTIR spectra revealed the urethane group N−H stretching (hydrogen-bonded) and −OH group absorption bands visible at 3250−3550 cm^{-1}, and N−H out-of-plane bending vibrations combined with C−N stretching at 1528−1542 cm^{-1}. The peaks identified as CH_2 and CH_3 were at 2855−2955 cm^{-1}. The absorption peaks observed between 1707 and 1726 cm^{-1} were attributed to the stretching vibrations of the NH−CO−O groups, both in their free and hydrogen-bonded forms.[31−33] Additionally, two characteristic peaks at 1139 and 1074 cm^{-1} indicated the presence of Si−O−Si and Si−O−C groups, respectively.[34] The emergence of bands at 3350 and 1727 cm^{-1} indicated that the isocyanate groups (−NCO) in the prepolymers had reacted with the hydroxyl groups (−OH) to form urethane linkages (NH−CO−O). The FTIR spectra of PDMSU intermediate prepolymers displayed a distinctive peak at 2272 cm^{-1},

https://doi.org/10.1021/acsomega.3c08102
ACS Omega 2024, 9, 2884−2895

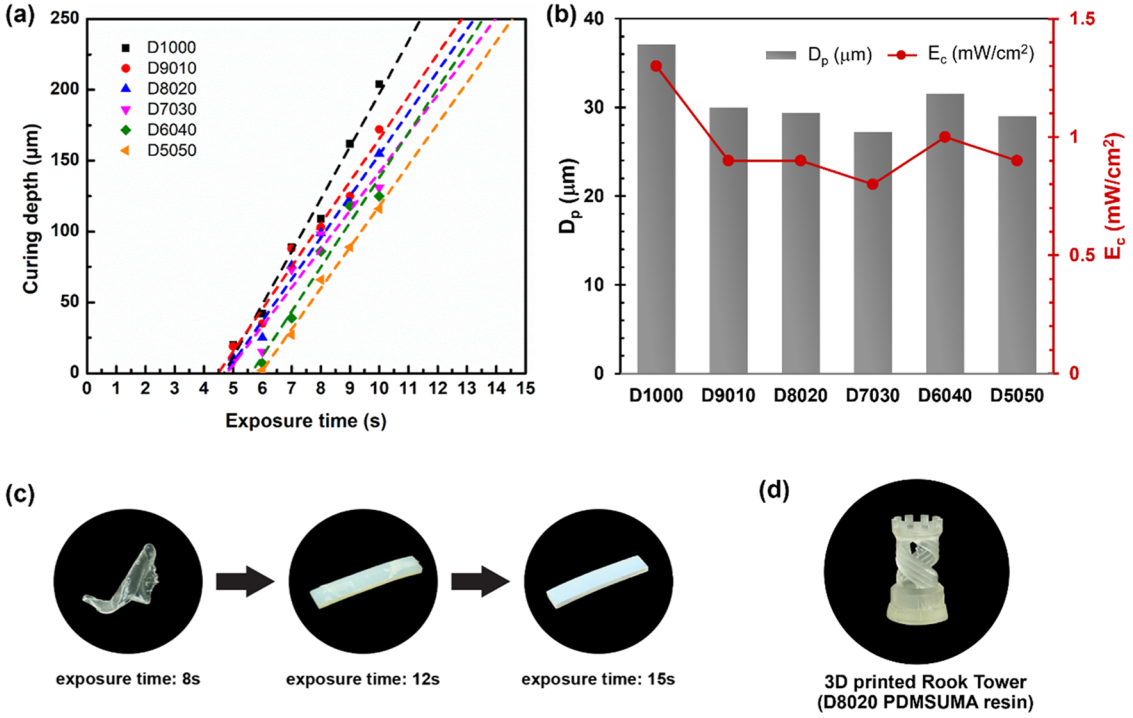

Figure 3. (a) Working curve of cure depth vs exposure time for the different PDMSUMA formulations. (b) Penetration depths (D_p) and the critical exposure (E_c) values of formulated PDMSUMA with varying cross-linker. (c) Test-printed samples obtained at different exposure times. (d) 3D-printed complex geometry (rook tower) using the D8020 PDMSUMA resin.

indicating the presence of an unreacted isocyanate. However, in PDMSUMA, this distinct peak was significantly diminished and nearly absent, signifying the successful reaction of NCO groups and hydroxyl groups.[32,33,35−37] Nevertheless, it is important to note that FTIR spectroscopy alone cannot definitively confirm the structural composition. Therefore, to establish a more comprehensive understanding and validate the existence of chemical bonds, NMR spectroscopy was employed for further investigations.

The chemical structures of PDMSU and PDMSUMA were also verified by ^{1}H NMR spectra as shown in Figure S1. The peaks at 0.06−0.26 ppm (A) were attributed to CH_2 groups of PDMS, while the peaks at 0.92−1.18 ppm (B), 1.51−2.07 ppm (C), 2.87−3.90 ppm (D), and 4.54−4.82 ppm (E) corresponded to IPDI.[38] For PDMSUMA, the ^{1}H NMR spectrum confirmed the attachment of methacrylates in PDMSU. The peaks at 0.03−0.22 ppm (A) were attributed to CH_2 groups of PDMS, while the peaks at 0.86−1.00 ppm (B), 1.65 ppm (C), 2.85−3.06 ppm (E), and 3.66−3.85 ppm (F) also corresponded to IPDI. New characteristic peaks were observed at 1.88 ppm (D) corresponded to the CH_2 group of HEMA in PDMSUMA. The CH_2 groups attached to the ester oxygen atom of HEMA (−COO−CH_2−CH_2−) were detected at 4.25 ppm (G), and the peaks at 5.53 and 6.08 ppm (H), (5.56−5.59 (C═CH_2, trans), 6.11−6.13 (C═CH_2, cis)), that were assignable to the existence of the methacrylate group in PDMSUMA.[33,39]

In addition, the ^{13}C NMR spectra of PDMSU are presented in Figure S2. The peaks at 0.08−0.95 ppm (A) were attributed to CH_2 groups of PDMS, while the peaks at 23.42−36.52 ppm (B), 44.47−57.01 ppm (C), 121.93 ppm (D), and 153.62 ppm (E) corresponded to IPDI.[40] For PDMSUMA, the ^{13}C NMR spectrum also confirmed the attachment of methacrylates in PDMSU. The peaks at 0.36−0.84 ppm (A) was attributed to CH_2 groups of PDMS, while the peaks at 23.22−31.78 ppm (C), 34.94−36.40 ppm (D), and 42.51−56.92 ppm (E) also corresponded to IPDI. The resonances of C═O groups were appearing at 155.56−156.78 and 167.30 ppm (I) due to the complete disappearance of N═C═O groups at 121.93 ppm. New characteristic peaks were observed at 18.12 ppm (B) for the CH_2 group of HEMA. The CH_2 groups attached to the ester oxygen atom of HEMA (−COO−CH_2−CH_2−) were detected at 60.91−66.38 ppm (F), and the peak at 121.7−126.05 ppm (G) and the peaks at 136.01 ppm (H) represented C═C, which were assignable to the existence of the methacrylate group in PDMSUMA.[34]

In summary, both the ^{1}H NMR and ^{13}C NMR spectra provide compelling experimental evidence regarding the chemical structures of PDMSU and PDMSUMA. The ^{1}H NMR spectrum exhibits resonances in the range of 4.54−4.82 ppm for PDMSU and 3.66−3.85 ppm for PDMSUMA, which correspond to the NH group. Furthermore, the ^{13}C NMR spectrum displays resonances at 153.62 ppm for PDMSU and 155.56 and 156.78 ppm, along with 167.30 ppm, for PDMSUMA, indicating the presence of the C═O group. These resonances unequivocally confirm the successful attachment of IPDI to PDMS and the subsequent attachment of methacrylates to PDMSU. Thus, the synthesis of the PDMSUMA oligomer was successfully accomplished. This corroborates the intended chemical modifications and establishes the desired structure of the PDMSUMA oligomer. The obtained NMR data provide robust and reliable evidence supporting the chemical characterization of the synthesized compounds.

3.2. Characterization of mSLA Printing Parameters.

The UV−vis absorbing ability of synthesized PDMSU and PDMSUMA was not responsive to the UV exposure range of the mSLA 3D printer, which is typically in the range of 385−

https://doi.org/10.1021/acsomega.3c08102
ACS Omega 2024, 9, 2884−2895

Table 2. Average Dimensional Data and Dimension Accuracy of 3D-Printed Specimens from Formulated PDMSUMA Resins

sample code	average length (mm)	length accuracy (%)	average width (mm)	width accuracy (%)	average thickness (mm)	thickness accuracy (%)
D1000	29.5 ± 0.1	98.2 ± 0.2	12.0 ± 0.1	99.6 ± 0.5	1.6 ± 0.1	81.5 ± 2.9
D9010	29.5 ± 0.1	98.3 ± 0.1	11.8 ± 0.1	98.4 ± 0.5	1.6 ± 0.1	80.5 ± 3.3
D8020	29.4 ± 0.1	98.0 ± 0.1	12.0 ± 0.1	99.7 ± 0.5	1.7 ± 0.1	84.5 ± 2.0
D7030	29.6 ± 0.1	98.6 ± 0.2	12.0 ± 0.1	99.9 ± 0.7	1.6 ± 0.1	82.0 ± 2.0
D6040	29.7 ± 0.1	98.9 ± 0.2	12.0 ± 0.1	99.8 ± 0.7	1.7 ± 0.1	84.5 ± 2.3
D5050	29.8 ± 0.1	99.2 ± 0.1	11.9 ± 0.1	99.4 ± 0.5	1.8 ± 0.1	88.5 ± 2.1

405 nm. Thus, the addition of a photoinitiator was necessary to promote the absorbing ability of PDMSUMA (illustrated in Figure S3).

In order to avoid print failures, having a low enough resin viscosity is essential for the build platform to move freely through the resin and for the resin to fill the small gap between the printed object and the bottom of the resin vat;[41] however, there is no standardized resin viscosity for optimum printability with mSLA 3D printing. However, the viscosity of most standard/rigid resins is 100−200 cps (25 °C), which belongs to the category of ultralow viscosity in 3D printing materials. The resin with a viscosity higher than 600 cps (25 °C) was categorized as a high-viscosity resin. The viscosity of ceramic suspensions could reach 5,000 cP, while the viscosity of some polymers with carbon nanocomposites could reach approximately 10,000 cP.[42] The high viscosity of synthesized PDMSUMA makes it inappropriate for mSLA 3D printing. Thus, PEGDMA was used as a reactive diluent, decreasing the viscosity of the synthesized PDMSUMA. The viscosities of the synthesized PDMSUMA and formulated PDMSUMA with PEGDMA are presented in Figure 2b (also demonstrated in Table S1). Adding PEGDMA at a concentration of 30 wt % provided a viscosity of approximately 250 cP, corresponding to the recommended viscosity for an acrylate-based resin used for 3D printing. To avoid any disruption in structural integrity that could potentially decrease the strength of the polymer, the amount of reactive diluent should be minimized.[43]

Reactive diluents, often acrylic monomers, can also participate in the cross-linking reaction and promote network structure formation. To control the cross-link density, a mixture of two different reactive diluents, including monofunctional HEMA and bifunctional PEGDMA, with varying weight ratios, was incorporated into the formulated PDMSUMA resin. The PDMSUMA and diluent were mixed in a fixed weight ratio of 70:30, while the PEGDMA and HEMA were mixed in varying weight ratios, including 100:0 (D1000), 90:10 (D9010), 80:20 (D8020), 70:30 (D7030), 60:40 (D6040), and 50:50 (D5050). The viscosities of all formulated PDMSUMA resins with varying PEGDMA and HEMA weight ratios were approximately 250 cP.

The suitable printing conditions for each formulated PDMSUMA resin were optimized by evaluating their photonic parameters and curing behavior using an mSLA system. The Jacobs equation, also known as the working curve, was employed as the fundamental model to describe the curing behavior of the prepolymers. The curing behavior was analyzed by measuring the exposure time from 1 to 10 s at a constant exposure intensity of 5 mW/cm^2, and the results were consistent with the working curve model. The model was represented by a dashed line, as shown in Figure 3a.

The penetration depths (D_p) of the different formulated PDMSUMA resins were also investigated and are presented in Figure 3b. It was found that D_p varied among the different formulations. The D1000 formulation without HEMA had the highest D_p of approximately 37 μm, while adding HEMA reduced the D_p of the formulated resins. The D_p values of D9010, D8020, and D5050 were similar, at approximately 30 μm. The D6040 formulation had a higher D_p value of approximately 32 μm, and the D7030 formulation had the lowest D_p value of approximately 27 μm. The differences in D_p can be attributed to various factors such as variations in the chemical composition, molecular weight, degree of cross-linking, and solubility of the polymers. Further studies may be necessary to fully understand the impact of these factors on the properties of the formulated PDMSUMA resins. The critical exposure (E_c) values of the different PDMSUMA formulations were also analyzed and are shown in Figure 3b. The results indicated that the E_c values varied from 0.80 to 1.02 mW/cm^2. The lowest E_c value was found in the D8020 formulation, while the D5050 formulation showed the highest E_c value. The differences in E_c values can be attributed to various factors such as the composition and viscosity of the formulation. A higher viscosity leads to a slower diffusion of the reactive species, reducing the polymerization rate and resulting in a higher E_c value. Further optimization of the printing parameters in term of exposure time was performed based on the determined values of critical exposure and penetration depth.

In addition, the suitable exposure time for each printing layer was optimized by maintaining consistent parameters, as detailed in Table 1 and thus fine tuning the suitable exposure time. As presented in Figure 3a, the minimum required maximum exposure time for curing a 50 μm layer thickness was approximately 8 s. However, during our actual printing operations at this exposure time, it was found that the printed layers did not consistently adhere together. To address this problem and ensure the successful printing of test specimens, the exposure time was increased to 15 s, especially for the most challenging resin formula. This adjustment significantly improved the binding strength between layers and allowed us to consistently achieve complete, high-quality prints for all of our testing specimens. The test-printed samples obtained from different exposure times and the example of 3D-printed complex geometry (rook tower) using the D8020 PDMSUMA resin are depicted in Figure 3c,d, respectively.

3.3. Characterizations of the 3D-Printed Formulated PDMSUMA Resins. *3.3.1. Dimension Accuracy.* The dimensional accuracy of the 3D-printed specimens was calculated according to eq 4. The dimensions of the CAD designed are 30 mm × 12 mm × 2 mm (length × width × thickness).

$$\text{dimension accuracy} = \frac{\text{average dimension of printed specimen}}{\text{dimension of CAD specimen}} \times 100\% \quad (4)$$

Table 2 displays the dimensions of the 3D-printed formulated PDMSUMA resins in terms of average length,

https://doi.org/10.1021/acsomega.3c08102
ACS Omega 2024, 9, 2884−2895

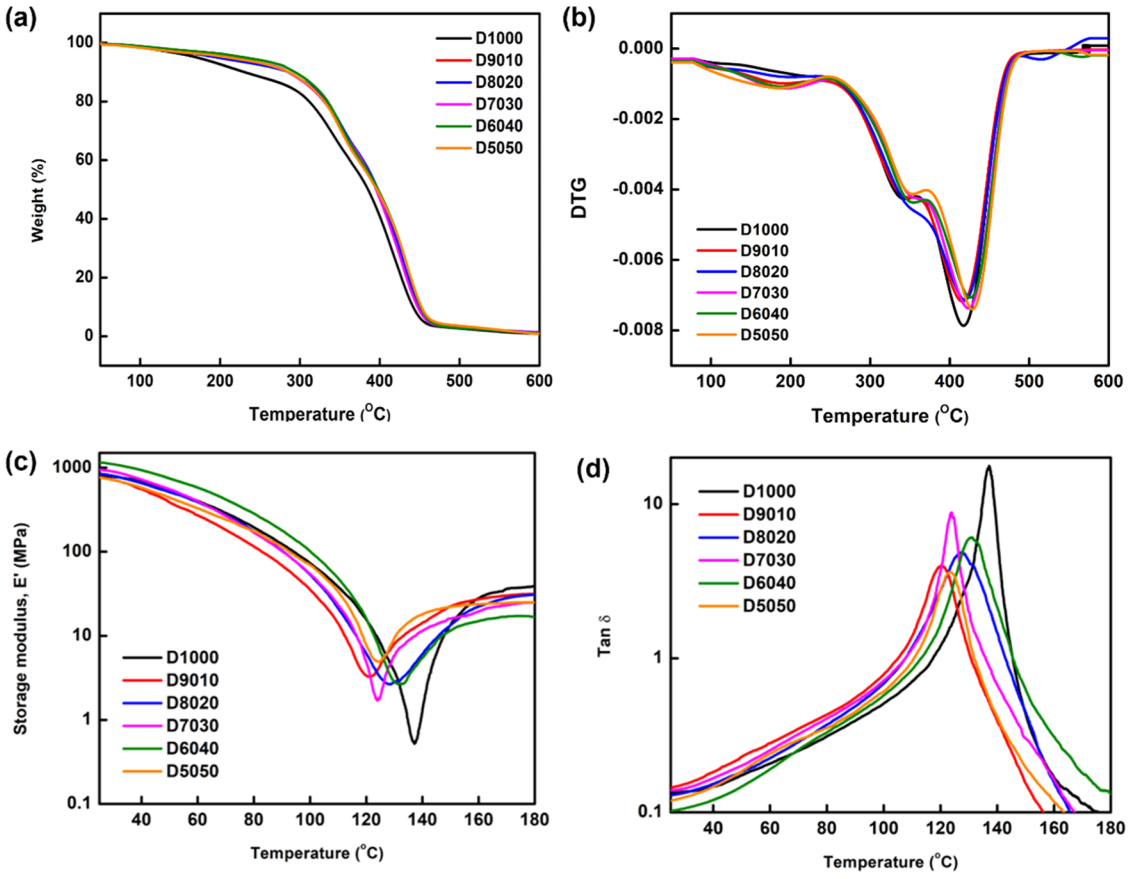

Figure 4. (a) Thermogravimetric analysis (TGA) curves. (b) Derivative thermogravimetric analysis (DTG) curves. (c) Storage modulus (E'). (d) Loss factor (tan δ) result from dynamic mechanical temperature sweep curves at a frequency of 5 Hz of the formulated PDMSUMA printed sample.

width, and thickness in millimeters along with their corresponding accuracy percentages. The length accuracy values indicate how close the measured length is to the actual length of the specimens. For instance, the length accuracy of D1000 was 98.2%, which implied that the measured length was, on average, 1.8% shorter than the actual length. Similarly, the width accuracy and thickness accuracy values indicate the degree of deviation from the actual width and thickness of the specimens. Regarding dimension accuracy, the findings demonstrated that all materials had relatively high accuracy percentages, ranging from 98.0 to 99.6%. This implied that the measured dimensions were relatively close to the actual dimensions of the specimens. However, it is noteworthy that the thickness accuracy is generally lower compared to the length and width, particularly for D5050, which has a thickness accuracy of 88.5%. This suggests that the thickness of the 3D-printed specimens is more susceptible to variations compared to the other dimensions. Normally, the thickness of the printed part may be lower than that of the CAD file due to the 3D printing conditions employed during the lamination process. In this study, the mSLA printing process involves a separation phase where the object being printed is detached from the bottom film of the resin vat. It is important to note that the tension created during this separation phase can have a significant impact on the overall lamination process for each layer, thus affecting the quality and accuracy of the printed object.[44]

3.3.2. Thermal Analysis. Figure 4a,b presents the TGA and DTG thermograms of the formulated PDMSUMA resins, respectively. The formulated PDMSUMA resins without HEMA (D1000) exhibited two decomposition stages. The first stage occurred around 300 °C and ended around 360 °C, while the second stage began at 370 °C and ended around 470 °C with 0.25% of residue. Weight loss between 300 and 380 °C can predominantly be ascribed to the decomposition of urethane bonds. Furthermore, the degradation of chain segments of polyols takes place, leading to the generation of volatile products, notably carbon dioxide.[45] The weight loss in the 400−470 °C range is attributed to the decomposition of cross-linking bonds and other chemical bonds or the oxidative decomposition of isocyanate compound.[45−48] In contrast, the thermograms of formulated PDMSUMA resins with HEMA (D9010, D8020, D7030, D6040, and D5050) showed a three-stage decomposition. The first decomposition stage was due to the degradation of HEMA in the copolymer backbone. Moreover, the formulated PDMSUMA samples obtained by 3D printing via photopolymerization (also known as radical polymerization) may contain some head-to-head (H−H) linkages. Some early decompositions occurring between 100 and 200 °C were attributed to the breakage of these linkages, as their bond dissociation energy was lower than that of C−C bonds, mainly due to the steric and inductive effects of vicinal ester groups.[49] The second and third decomposition stages were equivalent to the first and second decomposition stages of D1000 with around 1% residue, respectively. Related to the DTG thermogram, it can be observed that the second and third decomposition stages come closely in the D8020 sample, which may indicate a similar composition or dispersion of PDMSUMA, PEGDMA, and HEMA or a reaction occurring within the cross-linked polymer samples.

https://doi.org/10.1021/acsomega.3c08102
ACS Omega 2024, 9, 2884−2895

Table 3. Physical Properties of Formulated PDMSUMA Printed Samples

sample code	E' at 25 °C (MPa)	E'' at 25 °C (MPa)	T_g (crossover)	T_g (tan δ)	E' at T_g (MPa)	E'' at T_g (MPa)	gel content (%)
D1000	815.4 ± 3.1	108.9 ± 1.2	117.3 ± 0.7	137.2 ± 0.8	0.5 ± 0.1	9.2 ± 0.7	92.8 ± 1.6
D9010	771.5 ± 2.1	111.8 ± 1.0	105.3 ± 1.2	120.2 ± 1.0	3.3 ± 0.3	13.2 ± 0.7	93.4 ± 1.5
D8020	846.6 ± 3.2	109.5 ± 1.3	107.4 ± 0.8	127.6 ± 0.9	2.7 ± 0.3	13.1 ± 0.6	93.0 ± 2.3
D7030	946.2 ± 4.3	131.3 ± 0.7	107.7 ± 0.7	124.0 ± 0.8	1.7 ± 0.3	15.0 ± 0.6	92.7 ± 1.9
D6040	1160.8 ± 5.1	118.4 ± 0.9	113.2 ± 1.1	131.0 ± 1.0	2.7 ± 0.2	16.4 ± 0.8	92.8 ± 1.7
D5050	765.3 ± 2.3	91.1 ± 2.0	110.7 ± 0.9	123.2 ± 1.2	5.1 ± 0.4	18.5 ± 0.8	93.8 ± 1.3

3.3.3. Dynamic Mechanical Analysis (DMA) and Mechanical Properties. The mechanical properties of the 3D-printed formulated PDMSUMA samples were investigated by using DMA. The storage modulus and loss tangent (tan δ) curves with respect to temperature are shown in Figure 4c,d, respectively. This study demonstrated that the mechanical properties could be tailored by varying the cross-linker instead of focusing on the polymer matrix alone. The storage modulus and tan δ values of the different three-dimensional networks are mainly affected by the cross-link density. The reduction in the storage modulus curve and the peak of the tan δ curve indicate a structural phase transformation occurring from the relaxation of the polymer chains throughout the thermal transition. Thus, the magnitude of the tan δ can be used to predict the characteristic glass-transition temperature of materials.[50−52]

The storage modulus (E') reflects the elasticity or solidlike nature of materials and is used to determine their rigidity or ability to store energy. A high E' value implies greater elasticity, making the material more challenging to break down.[53,54] As shown in Figure 4c, the E' of the 3D-printed formulated PDMSUMA resins at room temperature ranged from 771.5 ± 2.1 to 1160.8 ± 5.1 MPa. As the temperature raised, the E' value decreased significantly and reached a minimum in the temperature range of 120−150 °C, associated with the softening effect of cross-linked polymers, which manifests itself in the glass-transition region and reaches to the rubbery state.[55] Specifically, this study focused on a novel type of silicone urethane methacrylate that exhibits shape memory properties upon being subjected to elevated temperatures. It is important to note that there is no prior literature available on the mechanical properties of these precisely synthesized materials. However, comparing to a study conducted by Singh et al.,[56] the formulated PDMSUMA resins exhibited mechanical properties (E') ranging from 765 to 1160 MPa, while the reference work by Singh et al. reported values ranging from 1070 to 2100 MPa. Despite this difference, it is important to emphasize that the formulated PDMSUMA resins distinguish themselves by their shape memory response at high temperatures. This characteristic could open intriguing possibilities for more specific applications.

PEGDMA increases the molecular weight between cross-links by reacting with methacrylate groups, forming a highly cross-linked network. However, excessive use of PEGDMA can lead to brittleness and reduced mechanical strength. On the other hand, HEMA increases T_g, making the 3D-printed specimens stiffer and more resistant to deformation at higher temperatures due to the formation of strong hydrogen bonds with methacrylate groups, resulting in a denser cross-linked network. To achieve optimal performance, finding the right balance between the concentrations of PEGDMA and HEMA is important.[43] The variations in the minimum storage modulus values of the cross-linked polymer can be attributed to differences in cross-link density, corresponding to the number of cross-link functionalities present. However, explaining the unexpected differences in storage modulus below T_g presents a more complex challenge. The storage modulus values at T_g with 5 replicates are documented in Table 3, and it becomes evident that the storage modulus shows an inverse trend compared to cross-link density below T_g. One possible explanation is the introduction of a monofunctional reactive diluent (HEMA), which increases the number of cross-link functionalities.[57] Due to its relatively small size and flexible structure, HEMA can also introduce some degree of chain flexibility.[58] This is why the network is likely to reduce the stiffness of the formulated PDMSUMA resins. Consequently, this helps explain the counteractive effect of cross-link density on the storage modulus at temperatures below T_g.

The peaks in the tan δ signals were identified as the glass-transition temperature (T_g). The T_g values of the PDMSUMA resin samples were 137.2 ± 0.8, 120.2 ± 1.0, 127.6 ± 0.9, 124.0 ± 0.7, 131.0 ± 1.0, and 123.2 ± 1.2 °C, respectively, as shown in Figure 4d. Adding HEMA led to a decrease in T_g, indicating that HEMA could bring more flexibility to the polymer network. In contrast, an increase in T_g corresponded to the rise of cross-link functionalities, leading to a higher cross-link density. Additionally, the van der Waals dispersion interactions between polymeric chains and hydrogen bonds between unmodified OH groups strongly influence the T_g of the cured polymer systems. The tan δ signal's shape also reflects the homogeneity of the network. A sharper and narrower signal indicates a more homogeneous network. The samples obtained from all formulated PDMSUMA resins showed a relatively narrow signal, suggesting a homogeneous network. The T_g decreases when the cross-link density is reduced. This is because the addition of HEMA, which is relatively small and flexible, increases the mobility of the polymer chains and introduces chain flexibility, as mentioned previously.

3.3.4. Shape Memory. The crossover points and the tan δ peak are two important characteristics of T_g that help determine the thermal and mechanical properties of materials. The crossover point is the temperature at which the storage and the loss modulus are equal. At this temperature, the material transitions from behaving more like an elastic solid ($E' > E''$) to behaving more like a viscous liquid ($E' < E''$). This temperature is an important reference point for determining the softening temperature and the onset of deformation. Alternatively, the tan δ peak is often used to determine the T_g of a material more accurately than by simply looking at the crossover point. It indicates the point of maximum energy dissipation, which can cause sample breakage during the experiment. The T_g determined from the crossover point and the tan δ peak is shown in Table 3.

The shape memory properties of the 3D-printed formulated PDMSUMA samples were characterized in terms of Rf and Rr, which were quantified through consecutive shape memory

https://doi.org/10.1021/acsomega.3c08102
ACS Omega 2024, 9, 2884−2895

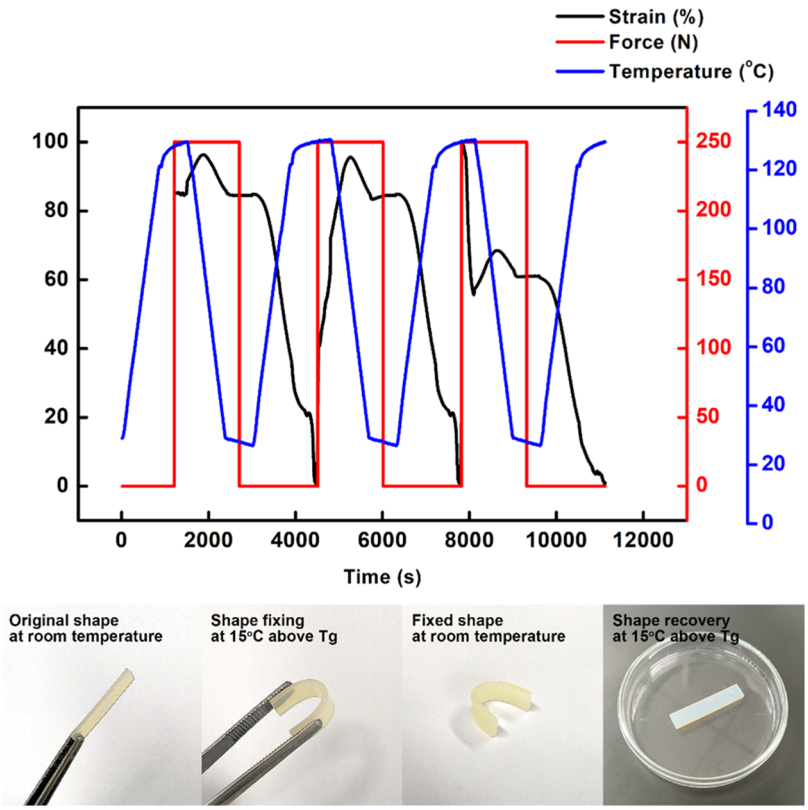

Figure 5. Two-dimensional demonstration of changes in strain, stress, and temperature with time in stress-controllable consecutive cyclic tensile shape memory processes of D8020 PDMSUMA resins.

cycles. Force-controlled cyclic thermal tests with a solid clamp were performed over three cycles (N = 1, 2, and 3). Ideally, Rf and Rr should be 100%, reflecting the perfect shape fixity and shape recovery. The formulated PDMSUMA resin samples exhibited different shape fixities and shape recovery due to the ratio of PEGDMA and HEMA compositions. Moreover, the strain percentage was normalized to facilitate calculation and to enhance comprehension. As shown in Figure 5, the Rf values for the three shape memory cycles for D8020 were 74.49%, indicating that the shape was almost completely fixed, and the results were consistent from one cycle to another. The Rr values for the three cycles were 100%, indicating complete shape recovery with a force of 250 N. However, when more HEMA was added to the diluent component, the results of D7030, D6040, and D5050 showed that the sample could not be fixed to a temporary shape and was unable to exhibit shape memory behavior. The Rf value decreases as the HEMA content increases due to the higher cross-link density of formulated PDMSUMA resin with HEMA. Since the shape memory effect is an entropic phenomenon, the chains become more closely restricted when the cross-link density increases, providing greater steric hindrance.[59] This inhibits the chains' ability to adopt the lowest entropy state, decreasing shape fixation. Regarding shape recovery, as the HEMA content increases, the Rr value increases due to the greater physical and chemical cross-link density. Polymers with a higher cross-link density have a greater elastic strain energy stored, which provides them with a higher driving force for subsequent thermally induced shape recovery. This is because the driving force responsible for shape recovery is, in fact, the residual stress introduced in the sample during the stretching process.[60−62] More results and analysis on the shape memory properties are demonstrated in the Supporting Information (Figures S4 and S5).

4. CONCLUSIONS

Silicone urethane methacrylate (PDMSUMA) resins were successfully synthesized, confirmed by Fourier transform infrared (FTIR) together with proton and carbon nuclear magnetic resonance (^{1}H NMR and ^{13}C NMR) spectroscopy techniques. The FTIR spectra showed the formation of urethane linkages through the reaction of isocyanate (NCO) with hydroxyl (OH) groups, while the ^{1}H NMR and ^{13}C NMR spectra confirmed the attachment of methacrylates in PDMSUMA. The effects of different PEGDMA and HEMA weight ratios in the formulated PDMSUMA resins, their photonic parameters, and the curing behavior were assessed. Adding a PEGDMA cross-linker as a reactive diluent decreases the viscosity of pure PDMSUMA to achieve the appropriate conditions for mSLA 3D printing. The results showed that the D_p and E_c values varied among the different formulations due to variations in the chemical composition, molecular weight, degree of cross-linking, and viscosity of the polymers. Based on the determined values of critical exposure and penetration depth, further optimization of the printing parameters was performed to enhance the quality of the printed specimens, as mentioned in Section 3.2. The dimensional accuracy of the printed specimens was calculated and found to be relatively high, with accuracy percentages ranging from 98.0 to 99.6% and 80.5 to 88.5% for thickness. The thermal analysis results revealed that the decomposition behavior of the formulated PDMSUMA resins varied depending on the presence or absence of HEMA and the cross-link density. A dynamic mechanical analysis (DMA) revealed that the cross-link density

https://doi.org/10.1021/acsomega.3c08102
ACS Omega 2024, 9, 2884−2895

was a crucial factor affecting the storage modulus and tan δ. Additionally, the shape memory properties of the 3D-printed formulated PDMSUMA samples with different ratios of PEGDMA and HEMA compositions were determined. The results showed that adding HEMA improves the shape memory behavior of the formulated PDMSUMA resin. The D8020, a formulated PDMSUMA resin with a mixed diluent, exhibited the optimal shape fixity and retained shape recovery with a force of 250 N for three consecutive cycles. However, as the HEMA content increased, the samples could not be fixed to a temporary shape and were unable to maintain the shape memory behavior. The study provides valuable insights into the formulation of PDMSUMA resins for developing shape memory materials with tailored properties. The formulated PDMSUMA resins with a T_g above 100 °C have potential applications in medical devices with superior thermal stability.

■ ASSOCIATED CONTENT

Supporting Information

The Supporting Information is available free of charge at https://pubs.acs.org/doi/10.1021/acsomega.3c08102.

Schematic of polymerization reaction and chemical structure of PDMSUMA, ^{1}H NMR spectra, ^{13}C NMR spectra, UV absorbance, and the shape memory test results of synthesized PDMSUMA resins (PDF)

■ AUTHOR INFORMATION

Corresponding Authors

Chuanchom Aumnate − *Metallurgy and Materials Science Research Institute, Chulalongkorn University, Bangkok 10330, Thailand; Center of Excellence in Responsive Wearable Materials, Chulalongkorn University, Bangkok 10330, Thailand;* orcid.org/0000-0003-4377-333X; Email: Chuanchom.a@chula.ac.th

Pranut Potiyaraj − *Department of Materials Science, Faculty of Science, Chulalongkorn University, Bangkok 10330, Thailand; Center of Excellence on Petrochemical and Materials Technology (PETROMAT) and Center of Excellence in Responsive Wearable Materials, Chulalongkorn University, Bangkok 10330, Thailand; Metallurgy and Materials Science Research Institute, Chulalongkorn University, Bangkok 10330, Thailand;* orcid.org/0000-0002-9114-9155; Email: Pranut.p@chula.ac.th

Author

Aphiwat Pongwisuthiruchte − *Department of Materials Science, Faculty of Science, Chulalongkorn University, Bangkok 10330, Thailand; Center of Excellence on Petrochemical and Materials Technology (PETROMAT), Chulalongkorn University, Bangkok 10330, Thailand*

Complete contact information is available at: https://pubs.acs.org/10.1021/acsomega.3c08102

Author Contributions

$^{\perp}$C.A. and P.P. contributed equally to this paper. A.P.: methodology, investigation, writing—original draft preparation; C.A.: conceptualization, methodology, data curation, writing—original draft preparation, writing—reviewing and editing; P.P.: resources, supervision, writing—reviewing and editing.

Notes

The authors declare no competing financial interest.

■ ACKNOWLEDGMENTS

The authors acknowledge the support from Thailand Science Research and Innovation Fund Chulalongkorn University and NSRF via the Program Management Unit of Human Resources & Institutional Development, Research and Innovation (grant no. B16F640115). Aphiwat Pongwisuthiruchte would like to acknowledge the Center of Excellence on Petrochemical and Materials Technology (PETROMAT) for the support. Additionally, the authors also would like to thank Metallurgy and Materials Science Research Institute (MMRI) for instrument and knowledge supporting.

■ REFERENCES

(1) Leng, J.; Lan, X.; Liu, Y.; Du, S. Shape-memory polymers and their composites: Stimulus methods and applications. *Prog. Mater. Sci.* **2011**, *56* (7), 1077−1135, DOI: 10.1016/j.pmatsci.2011.03.001.

(2) Hu, J.; Zhu, Y.; Huang, H.; Lu, J. Recent advances in shape−memory polymers: Structure, mechanism, functionality, modeling and applications. *Prog. Polym. Sci.* **2012**, *37* (12), 1720−1763, DOI: 10.1016/j.progpolymsci.2012.06.001.

(3) Meng, H.; Li, G. A review of stimuli-responsive shape memory polymer composites. *Polymer* **2013**, *54* (9), 2199−2221, DOI: 10.1016/j.polymer.2013.02.023.

(4) Huang, W. M.; Ding, Z.; Wang, C. C.; Wei, J.; Zhao, Y.; Purnawali, H. Shape memory materials. *Mater. Today* **2010**, *13* (7-8), 54−61, DOI: 10.1016/S1369-7021(10)70128-0.

(5) Wang, K.; Strandman, S.; Zhu, X. X. A mini review: Shape memory polymers for biomedical applications. *Front. Chem. Sci. Eng.* **2017**, *11* (2), 143−153, DOI: 10.1007/s11705-017-1632-4.

(6) Miao, S.; Castro, N.; Nowicki, M.; Xia, L.; Cui, H.; Zhou, X.; Zhu, W.; Lee, S. J.; Sarkar, K.; Vozzi, G.; et al. 4D printing of polymeric materials for tissue and organ regeneration. *Mater. Today* **2017**, *20* (10), 577−591, DOI: 10.1016/j.mattod.2017.06.005. From NLM PubMed-not-MEDLINE.

(7) Huang, W. M.; Yang, B.; Zhao, Y.; Ding, Z. Thermo-moisture responsive polyurethane shape-memory polymer and composites: a review. *J. Mater. Chem.* **2010**, *20* (17), 3367−3381, DOI: 10.1039/b922943d.

(8) Sun, L.; Huang, W. M. Thermo/moisture responsive shape-memory polymer for possible surgery/operation inside living cells in future. *Mater. Des. (1980−2015)* **2010**, *31* (5), 2684−2689, DOI: 10.1016/j.matdes.2009.11.036.

(9) Kim, J. S.; Lee, D. Y.; Koh, J. S.; Jung, G. P.; Cho, K. J. Component assembly with shape memory polymer fastener for microrobots. *Smart Mater. Struct.* **2014**, *23* (1), No. 015011, DOI: 10.1088/0964-1726/23/1/015011.

(10) Behl, M.; Kratz, K.; Zotzmann, J.; Nochel, U.; Lendlein, A. Reversible bidirectional shape-memory polymers. *Adv. Mater.* **2013**, *25* (32), 4466−4469, DOI: 10.1002/adma.201300880. From NLM Medline.

(11) Fernandes, R.; Gracias, D. H. Self-folding polymeric containers for encapsulation and delivery of drugs. *Adv. Drug Delivery Rev.* **2012**, *64* (14), 1579−1589, DOI: 10.1016/j.addr.2012.02.012. From NLM Medline.

(12) Zou, W.; Dong, J.; Luo, Y.; Zhao, Q.; Xie, T. Dynamic Covalent Polymer Networks: from Old Chemistry to Modern Day Innovations. *Adv. Mater.* **2017**, *29* (14), No. 1606100, DOI: 10.1002/adma.201606100.

(13) Zheng, N.; Fang, Z.; Zou, W.; Zhao, Q.; Xie, T. Thermoset Shape-Memory Polyurethane with Intrinsic Plasticity Enabled by Transcarbamoylation. *Angew. Chem.* **2016**, *128* (38), 11593−11597, DOI: 10.1002/anie.201602847. From NLM PubMed-not-MEDLINE.

(14) Zheng, N.; Hou, J.; Xu, Y.; Fang, Z.; Zou, W.; Zhao, Q.; Xie, T. Catalyst-Free Thermoset Polyurethane with Permanent Shape Reconfigurability and Highly Tunable Triple-Shape Memory Performance. *ACS Macro Lett.* **2017**, *6* (4), 326−330,

DOI: 10.1021/acsmacrolett.7b00037. From NLM PubMed-not-MEDLINE.
(15) Lendlein, A.; Kelch, S. Shape-Memory Polymers. *Angew. Chem., Int. Ed.* **2002**, *41* (12), 2034−2057, DOI: 10.1002/1521-3773(20020617)41:12<2034::AID-ANIE2034>3.0.CO;2-M.
(16) Abbasi, F.; Mirzadeh, H.; Katbab, A. A. Modification of polysiloxane polymers for biomedical applications: a review. *Polym. Int.* **2001**, *50* (12), 1279−1287.
(17) Perni, S.; Piccirillo, C.; Pratten, J.; Prokopovich, P.; Chrzanowski, W.; Parkin, I. P.; Wilson, M. The antimicrobial properties of light-activated polymers containing methylene blue and gold nanoparticles. *Biomaterials* **2009**, *30* (1), 89−93, DOI: 10.1016/j.biomaterials.2008.09.020. From NLM Medline.
(18) Bezuidenhout, D.; Williams, D. F.; Zilla, P. Polymeric heart valves for surgical implantation, catheter-based technologies and heart assist devices. *Biomaterials* **2015**, *36*, 6−25. From NLM Medline.
(19) Ceseracciu, L.; Heredia-Guerrero, J. A.; Dante, S.; Athanassiou, A.; Bayer, I. S. Robust and biodegradable elastomers based on corn starch and polydimethylsiloxane (PDMS). *ACS Appl. Mater. Interfaces* **2015**, *7* (6), 3742−3753, DOI: 10.1021/am508515z. From NLM Medline.
(20) McCoul, D.; Rosset, S.; Schlatter, S.; Shea, H. Inkjet 3D printing of UV and thermal cure silicone elastomers for dielectric elastomer actuators. *Smart Mater. Struct.* **2017**, *26* (12), No. 125022, DOI: 10.1088/1361-665X/aa9695.
(21) Zhou, L. Y.; Gao, Q.; Zhan, J. F.; Xie, C. Q.; Fu, J. Z.; He, Y. Three-Dimensional Printed Wearable Sensors with Liquid Metals for Detecting the Pose of Snakelike Soft Robots. *ACS Appl. Mater. Interfaces* **2018**, *10* (27), 23208−23217. From NLM PubMed-not-MEDLINE.
(22) Huang, P.; Xia, Z.; Cui, S. 3D printing of carbon fiber-filled conductive silicon rubber. *Mater. Des.* **2018**, *142*, 11−21, DOI: 10.1016/j.matdes.2017.12.051.
(23) Muth, J. T.; Vogt, D. M.; Truby, R. L.; Menguc, Y.; Kolesky, D. B.; Wood, R. J.; Lewis, J. A. Embedded 3D printing of strain sensors within highly stretchable elastomers. *Adv. Mater.* **2014**, *26* (36), 6307−6312, DOI: 10.1002/adma.201400334. From NLM PubMed-not-MEDLINE.
(24) Momeni, F.; M Mehdi Hassani N, S.; Liu, X.; Ni, J. A review of 4D printing. *Mater. Des.* **2017**, *122*, 42−79, DOI: 10.1016/j.matdes.2017.02.068.
(25) Choong, Y. Y. C.; Maleksaeedi, S.; Eng, H.; Wei, J.; Su, P. C. 4D printing of high performance shape memory polymer using stereolithography. *Mater. Des.* **2017**, *126*, 219−225, DOI: 10.1016/j.matdes.2017.04.049.
(26) Khoo, Z. X.; Teoh, J. E. M.; Liu, Y.; Chua, C. K.; Yang, S.; An, J.; Leong, K. F.; Yeong, W. Y. 3D printing of smart materials: A review on recent progresses in 4D printing. *Virtual Phys. Prototyping* **2015**, *10* (3), 103−122, DOI: 10.1080/17452759.2015.1097054.
(27) Melchels, F. P.; Feijen, J.; Grijpma, D. W. A review on stereolithography and its applications in biomedical engineering. *Biomaterials* **2010**, *31* (24), 6121−6130, DOI: 10.1016/j.biomaterials.2010.04.050. From NLM Medline.
(28) Nath, S. D.; Nilufar, S. An Overview of Additive Manufacturing of Polymers and Associated Composites. *Polymers* **2020**, *12* (11), 2719 DOI: 10.3390/polym12112719.
(29) Vazquez-Martel, C.; Becker, L.; Liebig, W. V.; Elsner, P.; Blasco, E. Vegetable Oils as Sustainable Inks for Additive Manufacturing: A Comparative Study. *ACS Sustainable Chem. Eng.* **2021**, *9* (49), 16840−16848, DOI: 10.1021/acssuschemeng.1c06784.
(30) Sultan, M.; Zia, K. M.; Bhatti, H. N.; Jamil, T.; Hussain, R.; Zuber, M. Modification of cellulosic fiber with polyurethane acrylate copolymers. Part I: Physicochemical properties. *Carbohydr. Polym.* **2012**, *87* (1), 397−404, DOI: 10.1016/j.carbpol.2011.07.070. From NLM PubMed-not-MEDLINE.
(31) *Ullmann's Encyclopedia of Industrial Chemistry*; Wiley, 2011; Vol. *40*.
(32) Alishiri, M.; Shojaei, A.; Abdekhodaie, M. J.; Yeganeh, H. Synthesis and characterization of biodegradable acrylated polyurethane based on poly(epsilon-caprolactone) and 1,6-hexamethylene diisocyanate. *Mater. Sci. Eng. C:* **2014**, *42*, 763−773, DOI: 10.1016/j.msec.2014.05.056. From NLM Medline.
(33) Chen, H.; Lee, S. Y.; Lin, Y. M. Synthesis and Formulation of PCL-Based Urethane Acrylates for DLP 3D Printers. *Polymers* **2020**, *12* (7), 1500 DOI: 10.3390/polym12071500.
(34) Kanai, T.; Mahato, T. K.; Kumar, D. Synthesis and characterization of novel silicone acrylate−soya alkyd resin as binder for long life exterior coatings. *Prog. Org. Coat.* **2007**, *58* (4), 259−264.
(35) Yeo, J. S.; Hwang, S. H. Synthesis of UV-Curable PDMS-Modified Urethane Acrylate Oligomer and Physical Properties of the Cured Film. *Elastomers Compos.* **2013**, *48* (4), 249−255, DOI: 10.7473/EC.2013.48.4.249.
(36) Zhao, T.; Yu, R.; Li, X.; Cheng, B.; Zhang, Y.; Yang, X.; Zhao, X.; Zhao, Y.; Huang, W. 4D printing of shape memory polyurethane via stereolithography. *Eur. Polym. J.* **2018**, *101*, 120−126, DOI: 10.1016/j.eurpolymj.2018.02.021.
(37) Xiong, T.; Zhang, Y. F. Synthesis and properties of polyurethane acrylate oligomer based on polycaprolactone diol. *e-Polymers* **2022**, *22* (1), 147−155, DOI: 10.1515/epoly-2022-0009.
(38) Prabhakar, A.; Chattopadhyay, D. K.; Jagadeesh, B.; Raju, K. V. S. N. Structural investigations of polypropylene glycol (PPG) and isophorone diisocyanate (IPDI)-based polyurethane prepolymer by 1D and 2D NMR spectroscopy. *J. Polym. Sci., Part A: Polym. Chem.* **2005**, *43* (6), 1196−1209.
(39) Tzeng, J. J.; Hsiao, Y. T.; Wu, Y. C.; Chen, H.; Lee, S. Y.; Lin, Y. M. Synthesis, Characterization, and Visible Light Curing Capacity of Polycaprolactone Acrylate. *BioMed Res. Int.* **2018**, *2018*, No. 8719624, DOI: 10.1155/2018/8719624. From NLM.
(40) Chen, X.; Liu, X.; Lei, J.; Xu, L.; Zhao, Z.; Kausar, F.; Xie, X.; Zhu, X.; Zhang, Y.; Yuan, W. Z. Synthesis, clustering-triggered emission, explosive detection and cell imaging of nonaromatic polyurethanes. *Mol. Syst. Des. Eng.* **2018**, *3* (2), 364−375. DOI: 10.1039/C7ME00118E.
(41) Mondal, D.; Haghpanah, Z.; Huxman, C. J.; Tanter, S.; Sun, D.; Gorbet, M.; Willett, T. L. mSLA-based 3D printing of acrylated epoxidized soybean oil - nano-hydroxyapatite composites for bone repair. *Mater. Sci. Eng.: C* **2021**, *130*, No. 112456, DOI: 10.1016/j.msec.2021.112456.
(42) Luo, Y.; Le Fer, G.; Dean, D.; Becker, M. L. 3D Printing of Poly(propylene fumarate) Oligomers: Evaluation of Resin Viscosity, Printing Characteristics and Mechanical Properties. *Biomacromolecules* **2019**, *20* (4), 1699−1708.
(43) Bloomquist, C. J.; Mecham, M. B.; Paradzinsky, M. D.; Janusziewicz, R.; Warner, S. B.; Luft, J. C.; Mecham, S. J.; Wang, A. Z.; DeSimone, J. M. Controlling release from 3D printed medical devices using CLIP and drug-loaded liquid resins. *J. Controlled Release* **2018**, *278*, 9−23, DOI: 10.1016/j.jconrel.2018.03.026.
(44) Shin, S. H.; Kwon, J. S.; Shim, J. S.; Kim, J. E. Evaluating the Three-Dimensional Printing Accuracy of Partial-Arch Models According to Outer Wall Thickness: An In Vitro Study. *Materials* **2021**, *14* (22), 6734 DOI: 10.3390/ma14226734.
(45) Wang, C.; Chen, X.; Chen, J.; Liu, C.; Xie, H.; Cheng, R. Synthesis and characterization of novel polyurethane acrylates based on soy polyols. *J. Appl. Polym. Sci.* **2011**, *122* (4), 2449−2455.
(46) Jang, E. S.; Khan, S. B.; Seo, J.; Akhtar, K.; Choi, J.; Kim, K. I.; Han, H. Synthesis and characterization of novel UV-Curable PU-Si hybrids: Influence of silica on thermal, mechanical, and water sorption properties of polyurethane acrylates. *Macromol. Res.* **2011**, *19*, 1006−1013, DOI: 10.1007/s13233-011-1002-x.
(47) Hu, Y.; Liu, C.; Shang, Q.; Zhou, Y. Synthesis and characterization of novel renewable castor oil-based UV-curable polyfunctional polyurethane acrylate. *J. Coat. Technol. Res.* **2018**, *15* (1), 77−85.
(48) Corcuera, M. A.; Rueda, L.; Fernandez d'Arlas, B.; Arbelaiz, A.; Marieta, C.; Mondragon, I.; Eceiza, A. Microstructure and properties of polyurethanes derived from castor oil. *Polym. Degrad. Stab.* **2010**, *95* (11), 2175−2184, DOI: 10.1016/j.polymdegradstab.2010.03.001.

(49) Çekingen, S. K.; Saltan, F.; Yildirim, Y.; Akat, H. A novel HEMA-derived monomer and copolymers containing side-chain thiophene units: Synthesis, characterization and thermal degradation kinetics. *Thermochim. Acta* **2012**, *546*, 87−93.
(50) Yoo, H. J.; Lee, Y. H.; Kwon, J. Y.; Kim, H. D. Comparision of the properties of UV-cured polyurethane acrylates containing different diisocyanates and low molecular weight diols. *Fibers Polym.* **2001**, *2*, 122−128, DOI: 10.1007/BF02875324.
(51) Tey, J. N.; Soutar, A. M.; Mhaisalkar, S. G.; Yu, H.; Hew, K. M. Mechanical properties of UV-curable polyurethane acrylate used in packaging of MEMS devices. *Thin Solid Films* **2006**, *504* (1−2), 384−390.
(52) Athawale, V. D.; Kulkarni, M. A. Polyester polyols for waterborne polyurethanes and hybrid dispersions. *Prog. Org. Coat.* **2010**, *67* (1), 44−54.
(53) Menczel, J. D.; Prime, R. B. *Therm. Anal.Polym.: Fundam. Appl.*; John Wiley & Sons, 2009.
(54) Hadavand, B. S.; Najafi, F.; Saeb, M. R.; Malekian, A. Hyperbranched polyesters urethane acrylate resin:A study on synthesis parameters and viscoelastic properties. *High Perform. Polym.* **2017**, *29* (6), 651−662, DOI: 10.1177/0954008317696566.
(55) Shojaeiarani, J.; Bajwa, D. S.; Hartman, K. Esterified cellulose nanocrystals as reinforcement in poly(lactic acid) nanocomposites. *Cellulose* **2019**, *26* (4), 2349−2362.
(56) Singh, N.; Bakhshi, H.; Meyer, W. Developing non-isocyanate urethane-methacrylate photo-monomers for 3D printing application. *RSC Adv.* **2020**, *10* (72), 44103−44110. From NLM PubMed-not-MEDLINE.
(57) Bowman, C. N.; Kloxin, C. J. Toward an enhanced understanding and implementation of photopolymerization reactions. *AIChE J.* **2008**, *54* (11), 2775−2795.
(58) Li, L.; Lee, L. J. Photopolymerization of HEMA/DEGDMA hydrogels in solution. *Polymer* **2005**, *46* (25), 11540−11547, DOI: 10.1016/j.polymer.2005.10.051.
(59) Xie, T. Recent advances in polymer shape memory. *Polymer* **2011**, *52* (22), 4985−5000.
(60) Wu, X. L.; Kang, S. F.; Xu, X. J.; Xiao, F.; Ge, X. L. Effect of the crosslinking density and programming temperature on the shape fixity and shape recovery in epoxy−anhydride shape-memory polymers. *J. Appl. Polym. Sci.* **2014**, *131* (15), No. 40559, DOI: 10.1002/app.40559.
(61) Tcharkhtchi, A.; Abdallah-Elhirtsi, S.; Ebrahimi, K.; Fitoussi, J.; Shirinbayan, M.; Farzaneh, S. Some New Concepts of Shape Memory Effect of Polymers. *Polymers* **2014**, *6* (4), 1144−1163.
(62) Calvo-Correas, T.; Gabilondo, N.; Alonso-Varona, A.; Palomares, T.; Corcuera, M. A.; Eceiza, A. Shape-memory properties of crosslinked biobased polyurethanes. *Eur. Polym. J.* **2016**, *78*, 253−263.

https://doi.org/10.1021/acsomega.3c08102
ACS Omega 2024, 9, 2884−2895